


# Replicated stalagmite-inferred centennial- to decadal-scale monsoon precipitation variability in southwest China since the mid Holocene

The Holocene  
0(0) 1–9  
© The Author(s) 2013  
Reprints and permission:  
sagepub.co.uk/journalsPermissions.nav  
DOI: 10.1177/0959683612471986  
hol.sagepub.com  


Xiuyang Jiang,<sup>1</sup> Yaoqi He,<sup>2</sup> Chuan-Chou Shen,<sup>3</sup> Zhizhong Li<sup>1</sup> and Ke Lin<sup>3</sup>

## Abstract

A lack of agreement between stalagmite records of the centennial- to decadal-scale Asian summer monsoon (ASM) variability since the mid Holocene limited our understanding of forcings and the possible impacts on culture evolution. Here we present replicated high-resolution stalagmite  $\delta^{18}\text{O}$  profiles from Dark Cave in Guizhou province, southwest China, established with 512 oxygen isotope data and 28  $^{230}\text{Th}$  ages, providing a continuous history of the ASM precipitation from 6100 to 300 years before present (yr BP, before AD 1950). Consistency of stalagmite  $\delta^{18}\text{O}$ -inferred long-term decreasing ASM trends since the mid Holocene between caves at this site and others in the Indian and East Asian monsoon realms on orbital timescales supports the effect of primary orbital solar forcings on monsoonal precipitation. The Dark Cave records display significant centennial- to decadal-scale variations, more evident than previous stalagmite records. Spectral analysis of the Dark Cave  $\delta^{18}\text{O}$  time series yields periodicities of 731–723, 281, 91–83, 67, and 55–54 yr, implying ASM intensity for the last 6 kyr could be associated with solar activity and variability of El Niño-Southern Oscillation.

## Keywords

$^{230}\text{Th}$  ages, Asian summer monsoon, Dark Cave, Holocene, stalagmite  $\delta^{18}\text{O}$ , weak Asian summer monsoon periods

Received 15 May 2012; revised manuscript accepted 26 November 2012

## Introduction

It has been suggested that civilizations and economic development of modern human societies in the eastern world, such as China and India, are closely linked to changes in the Asian Monsoon (AM) during the Holocene (e.g. Sinha et al. 2011; Tan et al., 2011; Zhang et al., 2008). Recent studies using a variety of AM proxy archives have led to significant advances in understanding of Holocene AM dynamics (e.g. An et al., 2000; Dykoski et al., 2005; Fleitmann et al., 2003, 2004; Gupta et al., 2003; He et al., 2004; Hong et al., 2005; Jiang et al., 2006; Jung et al., 2004; Neff et al., 2001; Wang et al., 2005; Yancheva et al., 2007). Stalagmites, one of natural archives, have advantages of possible absolute and high-precision chronology and abundant proxies. Thus, researchers have used stalagmites to reconstruct the history of AM variability during the Holocene (Dykoski et al., 2005; Fleitmann et al., 2003, 2004, 2007; Hu et al., 2008; Neff et al., 2001; Wang et al., 2005; Zhang et al., 2008).

Stalagmite records from locations between  $12^\circ$  and  $33^\circ\text{N}$  in the Asian continent document a general decreasing trend in the Asian summer monsoon (ASM) intensity, which is in agreement with millennial-scale insolation changes, supporting the connection between tropical/subtropical monsoons and orbital forcing (Cai et al., 2010; Dong et al., 2010; Fleitmann et al., 2003; Hu et al., 2008; Jiang et al., 2012; Wang et al., 2005). Except for some global events, such as 9.2 ka and 8.2 ka events (Cheng et al., 2009; Dykoski et al., 2005; Fleitmann et al., 2008; Shao et al., 2006), centennial- to decadal-scale ASM variability is not consistent between records (Overpeck and Cole, 2008); therefore, limiting our understanding of natural forcings on these timescales. This lack of agreement highlights the need for high quality climate records for the Holocene capable of resolving centennial- to decadal-scale variability.

Here, we present a new high-resolution and  $^{230}\text{Th}$ -dated ASM time series from two Holocene stalagmites collected from Dark Cave in the northern Guizhou Province of China. We use these replicate records to characterize centennial- to millennial-scale ASM variations and then we investigate the climate forcings and mechanisms of the ASM during the mid to late Holocene.

## Site and regional climatic settings

Dark Cave is located in Zhongxin, ~35 km northeast of Qianxi City, Guizhou Province, Southwest China ( $106^\circ 10'\text{E}$ ,  $27^\circ 12'\text{N}$ ) (Figure 1). This 10 km long cave, with only one entrance at an elevation of 1120 m, is approximately 270 km northwest of Dongge Cave and 550–600 km southwest of Heshang Cave and Sanbao Cave (Figure 1). A 30–50 cm thick layer of soil overlies the top of the cave and is mainly composed of yellow and calcareous soils. These soils support well-developed vegetation that consists of subtropical broadleaf evergreen and deciduous mixed forests.

<sup>1</sup>Fujian Normal University, China

<sup>2</sup>Guizhou Minzu University, China

<sup>3</sup>National Taiwan University, Taiwan

## Corresponding author:

Xiuyang Jiang, College of Geography Science, Fujian Normal University, No.32, Shangsang Road, Fuzhou, Fujian province, Fuzhou 350007, China.  
Email: xyjiang@fjnu.edu.cn

Chuan-Chou Shen, HISPEC, Department of Geosciences, National Taiwan University, Taipei 10617, Taiwan.  
Email: river@ntu.edu.tw.

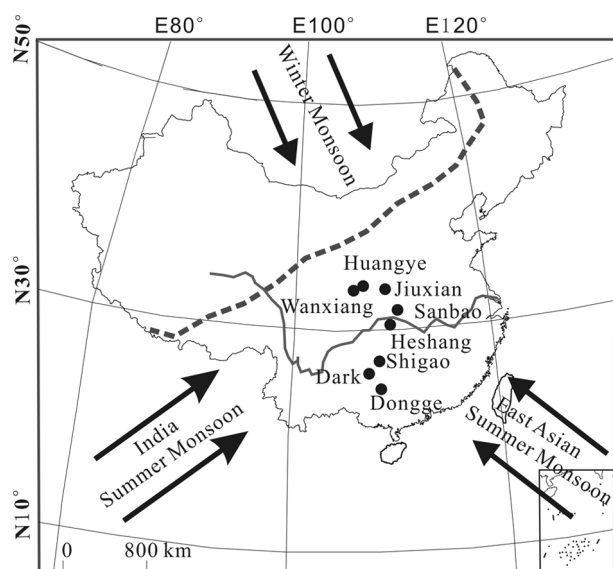


**Figure 1.** Map of mainland China with Chinese caves, including Dark Cave (this study), Wanxiang (Zhang et al., 2008), Huangye (Tan et al., 2011), Jiuxian Cave (Cai et al., 2010), Sanbao Cave (Dong et al., 2010), Heshang Cave (Hu et al., 2008), Shigao Cave (Jiang et al., 2012), and Dongge (Wang et al., 2005). The thick dashed line denotes the modern northwestern limit of the EASM.

The climate in our study area is a typical subtropical monsoon climate that is characterized by two distinct seasons: (1) a warm wet summer (May–September) when the intertropical convergence zone (ITCZ) lingers over south central China and (2) a cold dry winter (October–April) when the Siberian high is pronounced over Asia and the ITCZ migrates south. The mean annual precipitation is ~1050 mm and the mean annual temperature is 14°C, as recorded at the nearest meteorological station in Zuiyi, 80 km from Dark Cave. Temperature records spanning 50 years (AD 1950–2000) from this station reveals temperature varies between 2°C in the winter and 22°C in the summer. Cave temperature is a constant 13.5°C year around.

## Samples and methods

Two stalagmites, D1 and D2, were collected 3.5 km from the entrance of Dark Cave in October 2010. The stalagmites were halved and polished (Figure 2). X-ray diffraction analyses reveal that the two stalagmites were composed of calcite. No visible hiatus or porous structure was found on the polished surface. Stalagmite D1 is 340 mm in height and 8 cm in diameter, and D2 is 220 mm in height and 8 cm in diameter (Figure 2). For U-Th dating, 28 subsamples of 80–100 mg each were drilled from different layers in stalagmites D1 and D2 on a class-100 clean bench in a class-10,000 clean sampling room to avoid possible contamination (Shen et al., 2008). Subsamples were spiked with a triple-spike  $^{229}\text{Th}$ - $^{233}\text{U}$ - $^{236}\text{U}$  tracer for U-Th chemistry (Shen et al., 2003). U-Th isotopic compositions and concentrations were determined on a Thermo-Fisher NEPTUNE Multi-collection inductively coupled plasma mass spectrometer (MC-ICP-MS) at the High-Precision Mass Spectrometry and Environment Change Laboratory (HISPEC), Department of Geosciences, National Taiwan University (Frohlich et al., 2009; Shen et al., 2012). Instrumental background, mass fractionation, and procedural blanks were corrected and U-Th isotopic compositions and  $^{230}\text{Th}$  dates were determined using an offline data reduction process, which was modified from Shen et al. (2002). All date errors given are two standard deviations ( $2\sigma$ ) unless otherwise noted.

For  $\delta^{18}\text{O}$  analysis, a total of 512 powdered subsamples of 50–100  $\mu\text{g}$  each were extracted at 1 mm intervals along the central growth

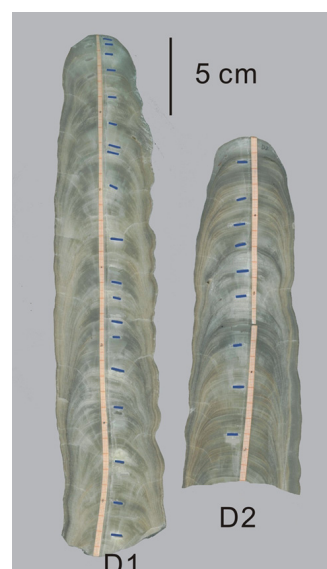


**Figure 2.** Photographs of two stalagmites D1 and D2 collected from Dark Cave. Samples of 1–1.5 mm in width were drilled for  $^{230}\text{Th}$  dating (blue bars). Powdered samples with a spatial resolution of 1 mm were extracted along the central growth axis on the polished surface for  $\delta^{18}\text{O}$  analysis (along tape in photographs) (colour figure available online).

axis on the polished surface using a carbide dental bit with a 0.5 mm diameter. Determination of oxygen isotopic composition was performed using a Thermo-Fisher MAT-253 mass spectrometer coupled with a Thermo-Fisher Gasbench II at the College of Geography Science, Fujian Normal University. Long-term 1-sigma reproducibility of the  $\delta^{18}\text{O}$  determinations using the international standard, NBS-19, is  $\pm 0.08\%$ . Carbonate stable isotope data are reported relative to the Vienna Pee Dee Belemnite (VPDB) standard.

## Results and discussion

### Chronology

The U-Th isotopic compositions and  $^{230}\text{Th}$  dates for samples extracted from the stalagmites D1 and D2 are given in Table 1. For stalagmite D1,  $^{238}\text{U}$  content ( $[^{238}\text{U}]$ ) is 300–600 ppb and  $[^{232}\text{Th}]$  ranges between 100 and 1600 ppt. Uncertainty of corrected  $^{230}\text{Th}$  dates ranges from  $\pm 7$  to  $\pm 44$  yr, except for a large error of  $\pm 118$  yr for subsample D1-40 with a high detrital  $[^{232}\text{Th}]$  of 12613 ( $\pm 37$ ) ppt (Table 1). For stalagmite D2,  $[^{238}\text{U}]$  is 300–600 ppb and  $[^{232}\text{Th}]$  ranges between 152 and 776 ppt.  $^{230}\text{Th}$  dates are yielded with a precision of  $\pm 9$ –33 yr, except for D2-15, which has a high detrital  $[^{232}\text{Th}]$  of 5590 ( $\pm 20$ ) ppt and a dating precision of  $\pm 69$  yr.

All  $^{230}\text{Th}$  dates are all in stratigraphic order. The  $^{230}\text{Th}$  dates reveal that stalagmite D1 deposited from 5486 ( $\pm 44$ ) to 325 ( $\pm 27$ ) yr BP (Table 1) that equates to deposition rates of 0.020–0.194 mm/yr. Stalagmite D2 deposited from 6127 ( $\pm 33$ ) to 1166 ( $\pm 69$ ) yr BP with deposition rates of 0.018–0.096 mm/yr. A linear interpolation between  $^{230}\text{Th}$  dates (yr BP, before AD 1950) and an algorithm method, StalAge (Scholz and Hoffmann, 2011), were used to establish age models. The age–depth relationship for the two stalagmites is plotted in Figure 3. The results show there is no significant difference between two chronologies, typically <10 years for stalagmite D1 and <30 years for D2. The only exception is the uppermost part of stalagmite D2, possibly caused by few  $^{230}\text{Th}$  dates and/or unidentified growth hiatus. The StalAge chronology, incorporating Monte Carlo simulation and Bayesian method (Scholz and Hoffmann, 2011), is used to build Dark Cave stalagmite  $\delta^{18}\text{O}$  sequences.

**Table 1.** U-Th isotopic compositions and  $^{230}\text{Th}$  dates for stalagmites D1 and D2 by MC-ICP-MS techniques at HISPEC, NTU.

Sample/depth (mm)	$^{238}\text{U}$ (ppb)	$^{232}\text{Th}$ (ppt)	$\delta^{234}\text{U}$ (measured)	$^{230}\text{Th}/^{238}\text{U}$ (activity)	Age/yr (uncorrected)	Age/yr BP (corrected)	$\delta^{234}\text{U}_{\text{initial}}$ (corrected)
D1-3	329.9±0.8	1439.9±6.7	1217.8±5.8	0.00886±0.00014	437±7	325±27	1219.1±5.8
D1-6	450.5±0.5	1093.1±10.4	1193.1±10.4	0.00880±0.00014	439±7	350±16	1193.2±2.9
D1-12	411.9±0.4	176.3±13.2	1196.9±3.1	0.00896±0.00014	446±7	381±7	1198.3±3.1
D1-23	408.1±0.3	628.2±14.7	1337.5±2.7	0.01164±0.00015	545±7	468±11	1339.5±2.7
D1-40	611.5±0.5	12613.0±36.8	1339.2±2.9	0.02321±0.00038	1088±18	795±118	1342.4±3.0
D1-57	503.0±0.6	821.7±10.3	1249.5±3.6	0.02757±0.00015	1345±8	1266±12	1254.2±3.7
D1-71	493.5±0.6	481.4±5.0	1285.0±3.4	0.03313±0.00013	1593±7	1522±9	1290.8±3.4
D1-76	457.7±0.5	98.8±6.1	1373.6±3.6	0.03959±0.00014	1834±7	1771±7	1380.8±3.6
D1-97	601.1±0.7	1377.6±8.1	1417.1±4.2	0.05054±0.00026	2303±13	2218±18	1426.2±4.2
D1-131	484.9±0.6	157.1±5.0	1351.1±3.3	0.05568±0.00015	2612±8	2548±8	1361.1±3.3
D1-159	537.1±1.3	237.6±8.0	1402.4±7.3	0.06888±0.00031	3168±17	3104±18	1415.0±7.4
D1-169	651.4±0.6	239.1±7.6	1448.9±2.9	0.07143±0.00021	3224±10	3160±11	1462.2±2.9
D1-185	464.6±0.4	1583.2±8.4	1439.6±2.7	0.08111±0.00049	3681±23	3584±29	1454.5±2.7
D1-195	562.9±0.6	214.4±8.3	1446.5±3.2	0.08179±0.00022	3702±11	3637±12	1461.7±3.2
D1-215	506.8±0.5	258.2±3.5	1402.5±2.8	0.08561±0.00021	3949±11	3883±11	1418.2±2.9
D1-240	630.3±0.7	542.1±12.6	1438.5±3.2	0.09271±0.00027	4218±14	4148±14	1455.7±3.2
D1-275	464.1±0.4	678.0±7.3	1237.0±2.8	0.09555±0.00027	4749±15	4672±17	1253.6±2.9
D1-301	298.5±0.3	157.3±7.3	1131.9±3.0	0.10047±0.00034	5250±20	5184±20	1148.8±3.1
D1-320	357.8±1.2	657.3±4.9	1161.1±10.9	0.10790±0.00061	5569±43	5486±44	1179.4±11.0
D2-15	469.5±0.7	5589.8±20.1	1382.0±4.3	0.02947±0.00040	1358±19	1166±69	1219.1±4.3
D2-38	496.1±0.5	249.5±6.3	1397.7±2.9	0.05503±0.00016	2530±8	2465±9	1386.8±2.9
D2-55	541.0±0.9	475.0±7.4	1413.5±4.9	0.06474±0.00022	2962±12	2892±13	1407.7±4.9
D2-68	571.6±1.2	193.7±3.9	1442.1±6.3	0.07058±0.00021	3194±13	3130±13	1425.3±6.4
D2-85	547.7±0.8	205.4±4.6	1438.0±4.1	0.08108±0.00021	3682±12	3618±12	1455.2±4.1
D2-101	625.7±1.0	373.2±9.5	1444.0±5.0	0.08496±0.00023	3851±13	3784±14	1453.0±5.0
D2-134	549.8±0.8	715.2±29.9	1463.6±4.7	0.10201±0.00043	4600±22	4526±23	1459.8±4.8
D2-160	386.5±0.6	152.4±5.6	1322.5±5.1	0.11250±0.00033	5398±20	5334±20	1482.7±5.2
D2-191	334.7±0.5	776.3±8.1	1212.4±4.3	0.12298±0.00054	6214±30	6127±33	1342.8±4.3

Notes: Analytical errors are  $2\sigma$  of the mean. Decay constant values are  $\lambda_{230}=9.1577\times 10^{-6}$  per yr,  $\lambda_{234}=2.8263\times 10^{-6}$  per yr (Cheng et al., 2000),  $\lambda_{238}=1.55125\times 10^{-10}$  per yr (Jaffey et al., 1971). Corrected  $^{230}\text{Th}$  age calculation, indicated in bold, is based on an assumed initial  $^{230}\text{Th}/^{232}\text{Th}$  atomic ratio of  $(4\pm 2)\times 10^{-6}$ . All corrected dates are presented in year before AD 1950.

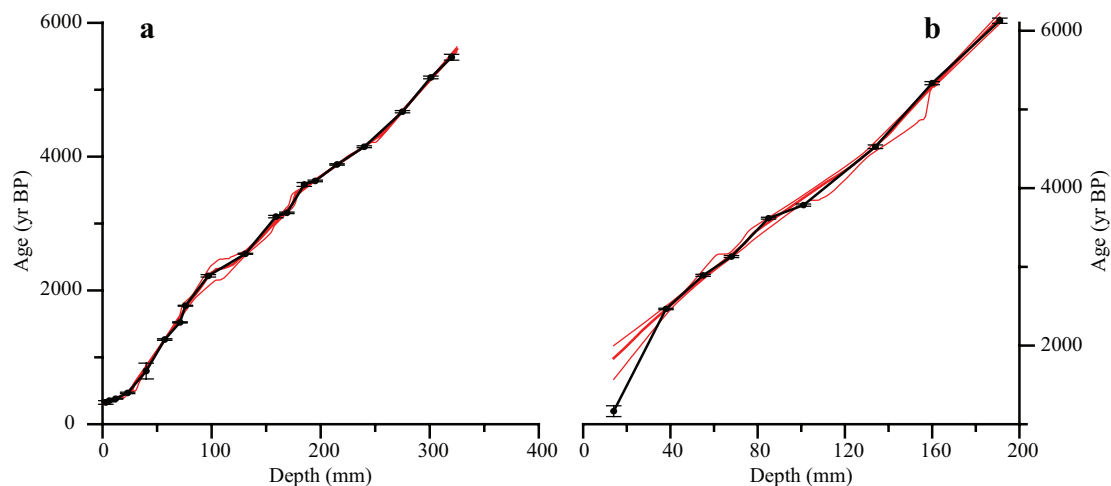


**Figure 3.** Chronologies for stalagmites (a) D1 and (b) D2 using a linear interpolation method (black) and StalAge model (red) (Scholz and Hoffmann, 2011) (colour figure available online).

## Oxygen isotopic records

The Hendy Test (Hendy, 1971) was performed in five individual laminae (three for D1, two for D2) and reveals a 1-sigma variability of  $\pm 0.03\text{--}0.06\text{‰}$  and the absence of significant correlations between  $\delta^{18}\text{O}$  and  $\delta^{13}\text{C}$  determinations (Figure 4). These results indicate that the calcite precipitated under oxygen isotopic equilibrium conditions. The replication test

between the two stalagmites found agreement between the contemporaneous  $\delta^{18}\text{O}$  variations from 5.5 to 1.8 kyr BP on decadal to millennial timescales (Figure 5). The robust replication test (Dorale and Liu, 2009) for equilibrium calcite deposition also provides evidence that insignificant kinetic fractionation occurred in these stalagmite records. A common environmental forcing resulted in the  $\delta^{18}\text{O}$  variations in these stalagmites.

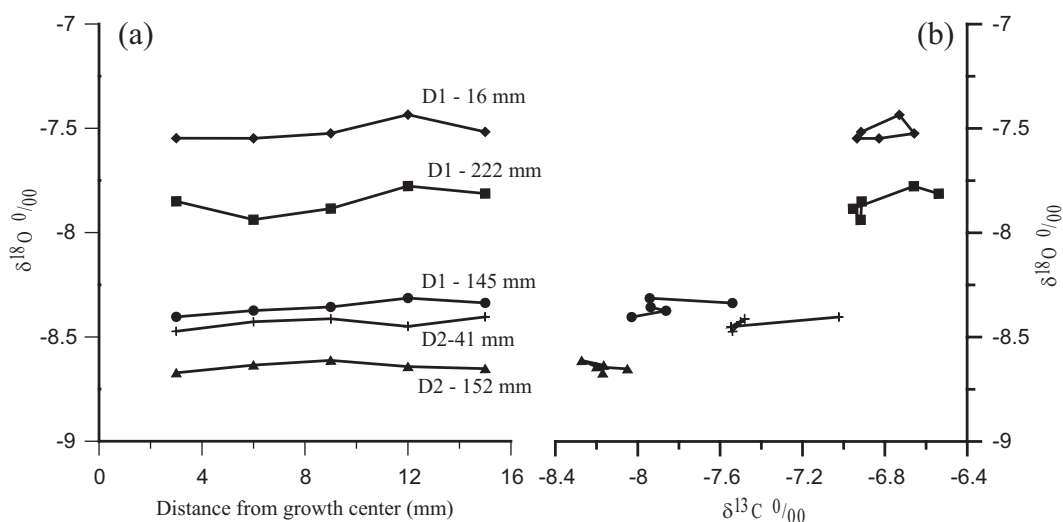


**Figure 4.** Results of the Hendy Test in five growth layers at depths from the stalagmite top of 16 mm, 145 mm and 222 mm for D1, and 41 mm and 152 mm for D2. (a) Variability within the growth layers varies between  $\pm 0.03$  and  $0.06\text{‰}$  for  $\delta^{18}\text{O}$ . (b) Cross-plot of  $\delta^{18}\text{O}$  and  $\delta^{13}\text{C}$  reveals the lack of a relationship between  $\delta^{18}\text{O}$  and  $\delta^{13}\text{C}$  determinations for each layer revealing insignificant kinetic fractionation thus indicating the stalagmites deposited under equilibrium conditions.

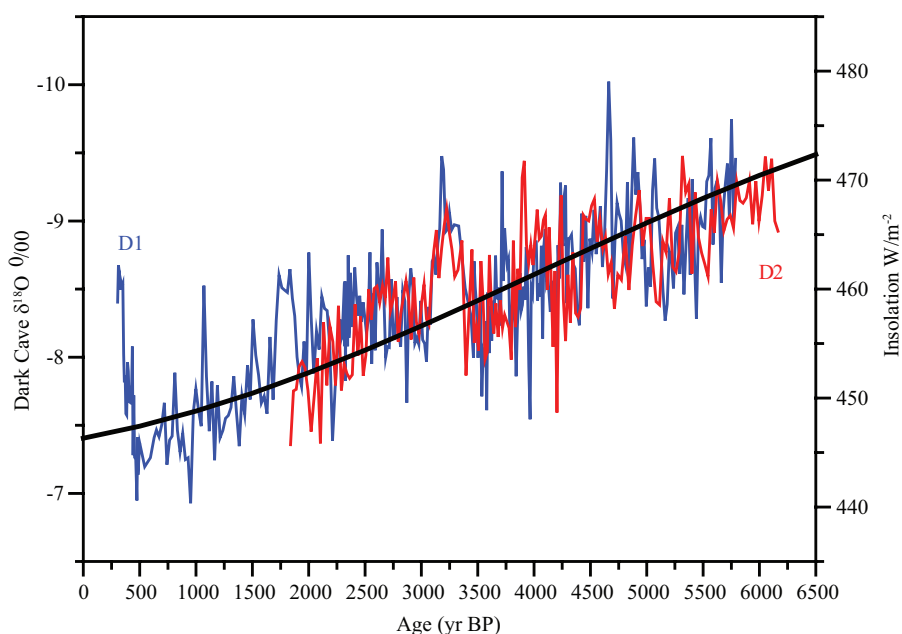


**Figure 5.** The  $\delta^{18}\text{O}$  time series for the Dark Cave stalagmites D1 (blue) and D2 (red) plotted with the insolation curve at  $30^\circ\text{N}$  (black) (colour figure available online).

Changes in stalagmite  $\delta^{18}\text{O}$  are controlled by climatic and environmental factors, including temperature and/or precipitation (Hendy, 1971). Previous studies of the Dongge Cave (Dykoski et al., 2005) and Wulu Cave (Liu et al., 2010) in the Guizhou Province suggest little temperature effect on stalagmite  $\delta^{18}\text{O}$ , leaving meteoric precipitation as the dominant factor. Meteorological data from a nearby meteorological station (Zuiyi,  $27^\circ 42'\text{N}$ ,  $106^\circ 52'\text{E}$ ; elevation=844 m, 80 km NE of Dark Cave) shows that 70–80% of the yearly precipitation falls in the summer (May–September). The  $\delta^{18}\text{O}$  of summer precipitation is  $-9.7\text{‰}$  (SMOW) which is  $-3.3\text{‰}$  lower than winter precipitation (IAEA/WMO, 2006).

A previous study demonstrated that the  $\delta^{18}\text{O}$  variation in a Chinese cave stalagmite varies with summer/winter rainfalls (Wang et al., 2001). As discussed in the study of Cheng et al. (2009), the low  $\delta^{18}\text{O}$  precipitation is associated with summer monsoon is attributed to a distant tropical Indo-Pacific source and the high  $\delta^{18}\text{O}$  precipitation for rest of the year is attributed to a

local source. The ratio of low- to high- $\delta^{18}\text{O}$  precipitation data correlates well with the absolute amount of low- $\delta^{18}\text{O}$  summer monsoon precipitation (Cheng et al., 2009). Therefore, Cheng et al. (2009) deduced that the Chinese stalagmite  $\delta^{18}\text{O}$  values represent ASM precipitation or ASM intensity. Based on modern climatic observations and previous Chinese stalagmite studies (Cai et al., 2010; Cheng et al., 2009; Dong et al., 2010; Dykoski et al., 2005; Liu et al., 2010; Tan et al., 2011; Jiang et al., 2012; Wang et al., 2005), we assume the stalagmite  $\delta^{18}\text{O}$  from Dark Cave is a qualitative proxy of ASM precipitation and intensity, with heavier values indicating a weak ASM, and vice versa.

Holocene stalagmite  $\delta^{18}\text{O}$  records in the AM territory are plotted in Figure 6. The overall trend in our stalagmite  $\delta^{18}\text{O}$  record varies from  $-9.5\text{‰}$  at 6.1 kyr BP to  $-6.9\text{‰}$  at 0.49 kyr BP and appears to follow summer insolation at  $30^\circ\text{N}$ , except for a short time window of 0.3–0.49 kyr BP (Figure 6). This trend is similar to the insolation at  $30^\circ\text{N}$  (Figure 6) in the mid to late Holocene

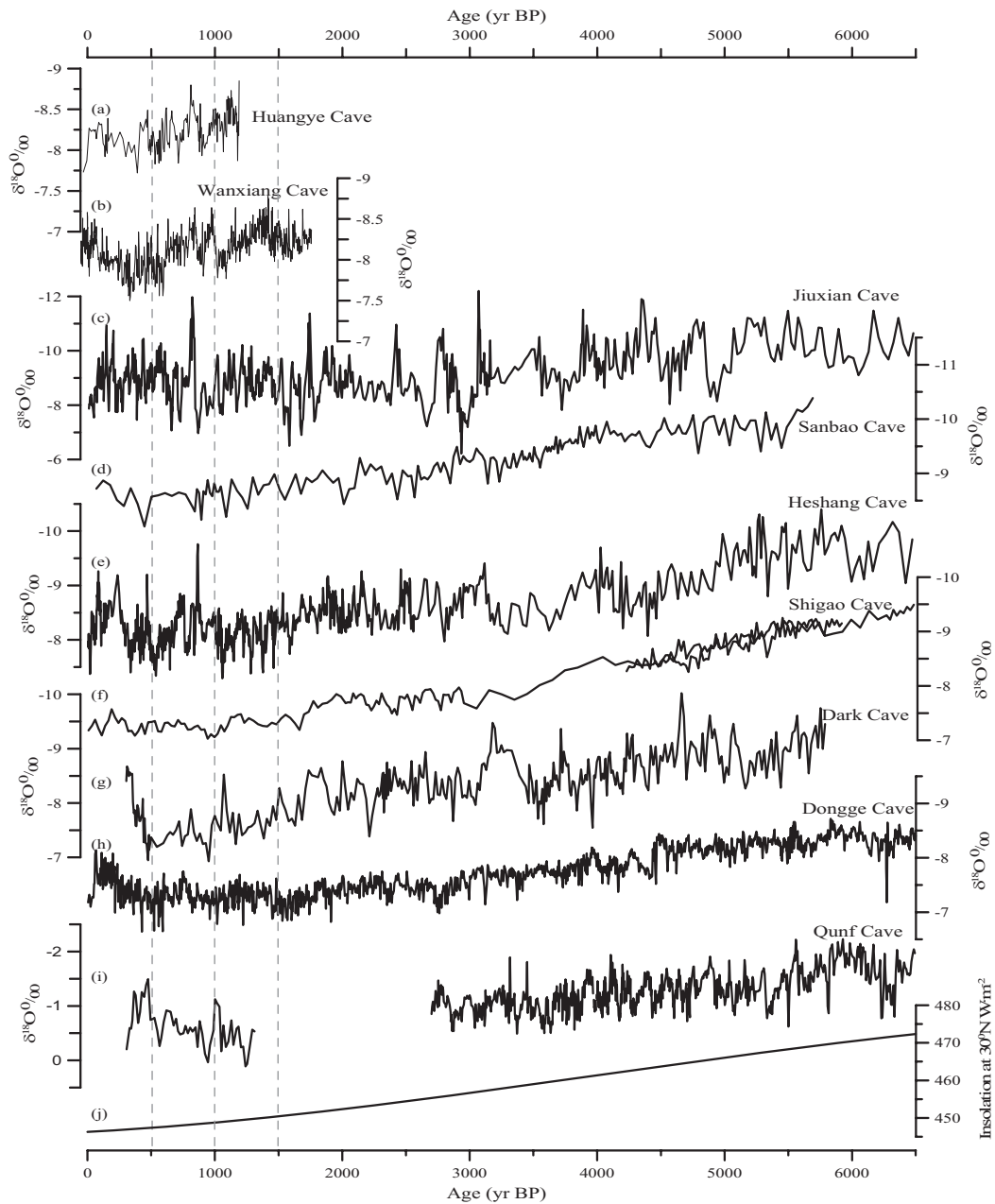


**Figure 6.** Comparison of stalagmite  $\delta^{18}\text{O}$  records from caves in (a) Huangye (Tan et al., 2011), (b) Wangxiang (Zhang et al., 2008), and (c) Jiuxian (Cai et al., 2010) in north China; (d) Sanbao (Dong et al., 2010) and (e) Heshang (Hu et al., 2008) in central China; (f) Shigao (Jiang et al., 2012), (g) Dark (this study) and (h) Dongge (Wang et al., 2005) in southwest China; (i) and Qunf in Southern Oman (Fleitmann et al., 2003). (j) Insolation at  $30^\circ\text{N}$  (Berger and Loutre, 1991).

and therefore supports the hypothesis (Kutzbach, 1981) that ASM intensity is primarily controlled by insolation.

### Consistency of Holocene trend between monsoonal precipitation records

The Indian and the East Asian monsoon (EAM) are two main sub-systems of the AM. High-resolution paleoclimate records of AM precipitation will allow us to investigate the relationship between Indian monsoon (IM) and EAM during the mid to late Holocene and better understand AM precipitation. We compare our records with other stalagmite records with similar high resolution and precise chronologies from both IM and EAM regions. For the IM, we examine records from Qunf, Oman ( $54^\circ18'\text{E}$ ,  $17^\circ10'\text{N}$ , Fleitmann et al., 2003). For the EAM, we examine records from

Wangxiang ( $105^\circ00'\text{E}$ ,  $33^\circ19'\text{N}$ , Zhang et al., 2008), Huangye ( $105^\circ7'\text{E}$ ,  $33^\circ35'\text{N}$ , Tan et al., 2011), Jiuxian ( $109^\circ6'\text{E}$ ,  $33^\circ34'\text{N}$ , Cai et al., 2010), Sanbao ( $110^\circ26'\text{E}$ ,  $31^\circ40'\text{N}$ , Dong et al., 2010) and Heshang ( $110^\circ25'\text{E}$ ,  $30^\circ27'\text{N}$ , Hu et al., 2008) from Central China in the EAM zone. For the region in southwest China with an influence by the IM and the EAM, we examine records from Shigao ( $107^\circ10'\text{E}$ ,  $28^\circ11'\text{N}$ , Jiang et al., 2012), Dongge ( $108^\circ5'\text{E}$ ,  $25^\circ17'\text{N}$ , Wang et al., 2005) and Dark Cave ( $106^\circ10'\text{E}$ ,  $27^\circ12'\text{N}$ , this study). All the stalagmite  $\delta^{18}\text{O}$  records examined exhibit increasing trends in  $\delta^{18}\text{O}$  similar to the trend in insolation at  $30^\circ\text{N}$  (Figure 6). The general consistency of monsoon records from  $17^\circ$  to  $33^\circ\text{N}$  indicates an in-phase relationship between IM and EAM on orbital timescales for the mid to late Holocene with the monsoon weakening in the late Holocene. Additionally, this weakening trend of summer monsoon intensity is observed in records of pollen, lake, and marine sediments at AM region (Gupta et al.,

2003; Jiang et al., 2006; Jung et al., 2004; Yancheva et al., 2007). All these records follow summer insolation at 30°N on orbital timescales, suggesting that the shift in the mean position of the ITCZ controls the summer monsoon precipitation throughout the entire mid- to low-latitude regions in Asia (Fleitmann et al., 2007), as supported by model simulations (e.g. Kutzbach, 1981).

We noticed that the absolute values of stalagmite  $\delta^{18}\text{O}$  records are different for the past 6 kyr (Figure 6). The  $\delta^{18}\text{O}$  values decrease from 0–3‰ at 17°N (Qunf Cave), and –6–10‰ at 25–28°N (Dark, Dongge, and Shigao Caves), to –7–12‰ at 30–33°N (Heshang, Sanbao, and Jiuxian Caves). This  $\delta^{18}\text{O}$  depletion northward is attributed to the latitude effect on isotopic fractionation of precipitation (Lachniet, 2009, and references therein). Furthermore, the amplitude of stalagmite  $\delta^{18}\text{O}$  changes over the past 6 millennia is 1.5‰ in Dark, Heshang and Qunf Caves, ~1.5‰ less than that in Jiuxian Cave and 0.5‰ higher than those in Dongge, Shigao, and Sanbao Caves (Figure 6). The difference could result from different local hydrological conditions and/or moisture sources (e.g., Cai et al., 2010; Dayem et al., 2010; Pausata et al., 2011).

### Asynchronicity of regional monsoonal dynamics in the recent five centuries

Despite the agreement on orbital timescales for a decreasing trend across the summer monsoon region, there is a striking asynchronicity of decreasing stalagmite  $\delta^{18}\text{O}$  records and their strengthened monsoon trends between stalagmites at IM and EAM territories for the last 500 years (Figure 6). The onset of this enhanced regional precipitation occurred at 490–550 yr BP for the IM region between 17° and 27°N (Qunf, Dongge, and Dark Caves). This observation is supported by the monsoon-induced marine upwelling record based on planktonic foraminifer *Globigerina bulloides* abundance data from the Arabian Sea, which indicates that southwest monsoon wind strength increased during the past four centuries (Anderson et al., 2002). The asynchronous onsets of this strong monsoon intensity occurred at 280 yr BP at 28–30°N (Shigao and Heshang Caves), 450 yr BP at 31°N (Sanbao Cave), 330–390 yr BP at 33°N (Huangye and Wanxiang Cave), and absent at Jiuxian Cave in EAM regions (Figure 6). This asynchronicity cannot be attributable to subsampling resolution or uncertainties of age chronologies built by  $^{230}\text{Th}$  dates with 2-sigma uncertainties of only <30 yr. In addition, the amplitude of this event generally decreased latitudinally, about 1‰ at 17–30°N (Qunf, Dongge, Dark, and Heshang Caves), 0.4–0.5‰ at 28–31°N (Shigao and Sanbao Caves), and 0–0.4‰ at 33°N (Jiuxian, Wanxiang, and Huangye Caves) (Figure 6). This phenomenon of regional differences in the precipitation responses has been speculated to be related to complexity of regional topography and atmospheric circulation by Tan et al. (2009). Other studies (e.g. Cheng et al., 2012; Dayem et al., 2010; Pausata et al., 2011) suggest that a moisture source change plays an important role in modulating stalagmite  $\delta^{18}\text{O}$  amplitude.

The observation of different enhancing trends of IM and EAM intensities during the last several centuries suggests a complicated mutual relationship (Tao and Chen, 1987). The IM is a typical tropical monsoon system, driven by a south–north ocean–land thermal gradient; a warming trend over the Eurasia for the past four centuries has enhanced the Indian (or southwest) monsoon, leading to the northward shift of ITCZ (Anderson et al., 2002). As a result, a decreasing  $\delta^{18}\text{O}$  trend is found at 490–550 yr BP in Qunf, Dongge, and Dark Caves at IM region. However, the EAM, dominated by both south–north and east–west ocean–land thermal gradients, is more complicated than the IM and its summer rainfall belt is influenced by the tropical trough (ITCZ) and the subtropical monsoon (Mei–Yu front) (Tao and Chen, 1987; Wang

and Lin, 2002). A giant North Pacific subtropical ridge develops because of the east–west thermal contrast, which separates and also couples the subtropical front rain belt to the tropical monsoon trough rain belt, forming a coupled tropical and subtropical monsoon system with a large meridional extent (Wang et al., 2003). Instrumental observation and historical climate records reveal strong spatial variations of rainfall distributions on annual to decadal scales over the EAM region (e.g. Guo et al., 2003; Liu et al., 2008; Zhang et al., 2010; and references therein). In general, as the East Asian summer monsoon (EASM) begins to increase, the Mei–Yu front will penetrate further north and bring more precipitation to northern China, southern China, and southeast coastal areas of Asia, whereas less rainfall occurs in the upper and middle reaches of the Yangze and Jiang–Huai drainage basins. A recent study by Liu et al. (2011) showed that the East Asian–North Indian Ocean index reveals an increasing EASM trend since AD 1620. The water vapor source for summer precipitation over the EAM territory is from the distant Indian Ocean and the adjacent tropical Indo–Pacific source, resulting in a complex relationship of rainfall amount and its  $\delta^{18}\text{O}$  value, as evidenced by the asynchronous timing of stalagmite  $\delta^{18}\text{O}$  change in EAM area for the past 500 years.

### Centennial- to decadal-scale monsoon precipitation recorded by stalagmite $\delta^{18}\text{O}$ records

The high-resolution stalagmite  $\delta^{18}\text{O}$  records for the past 6.1 kyr from caves of Dark (D1 and D2), Dongge (DA), and Heshang (HS-4) are plotted in Figure 7. All stalagmite  $\delta^{18}\text{O}$  records exhibit centennial- to decadal-scale oscillations, suggesting that these changes are intrinsic characteristics of the AM in the Holocene. The Dark Cave  $\delta^{18}\text{O}$  records display clear centennial-scale variations that are more evident than other records (Figure 7). This suggests that Dark Cave is more sensitive to the ASM rainfall than other locations in our comparison.

The Holocene ice-rafted debris (IRD) events (named Bond Events) were first identified in the North Atlantic marine records (Bond et al., 1997) and have been documented in global terrestrial and marine records (Wanner et al., 2011). Four weak monsoon (WM) periods, >100 years, with high  $\delta^{18}\text{O}$  values and amplitudes of 0.5–1.5‰, centered between abrupt transitions of  $\delta^{18}\text{O}$  values at 4.2, 2.8, 1.6, and 0.5 kyr BP in both D1 and D2 records, are coherent with Bond Events, 0–3 (Figure 7, Bond et al., 1997). These WM periods also match ones in previous stalagmite  $\delta^{18}\text{O}$  records (Hu et al., 2008; Wang et al., 2005) (Figure 7). This consistency supports the previous idea of the teleconnection relationship between low-latitude AM and high-latitude climate conditions on centennial to decadal timescales during the Holocene (Gupta et al., 2003; Wang et al., 2005).

Stalagmite D1 and D2 time series from Dark Cave reveals a double-peak WM period from 4.4 to 4.1 kyr BP, which is also recorded in Dongge Cave and Heshang Cave within dating error (Figure 7). This 4.2 ka period is reported as a cold event in other locations in China (An et al., 2005; Wu and Liu, 2004). This prolonged drought period is associated with diminished monsoonal intensity and likely triggered the collapse of Neolithic cultures in China (An et al., 2005).

The Dark Cave records captured an abrupt and severe decrease in summer monsoon intensity between 3.7 and 3.4 kyr BP (Figure 7). The timing and pattern of this 3.5 ka WM period is strikingly similar to that recorded in stalagmite HS-4 of Heshang Cave. This WM period is poorly expressed in the Dongge DA record, but clearly shown in a stalagmite D4 record (Dykoski et al., 2005) from the same cave. The signal of stalagmite DA or D4 could be clouded by complicated cave hydrological processes (Overpeck and Cole, 2008). The absence of its counterpart Bond Event in the

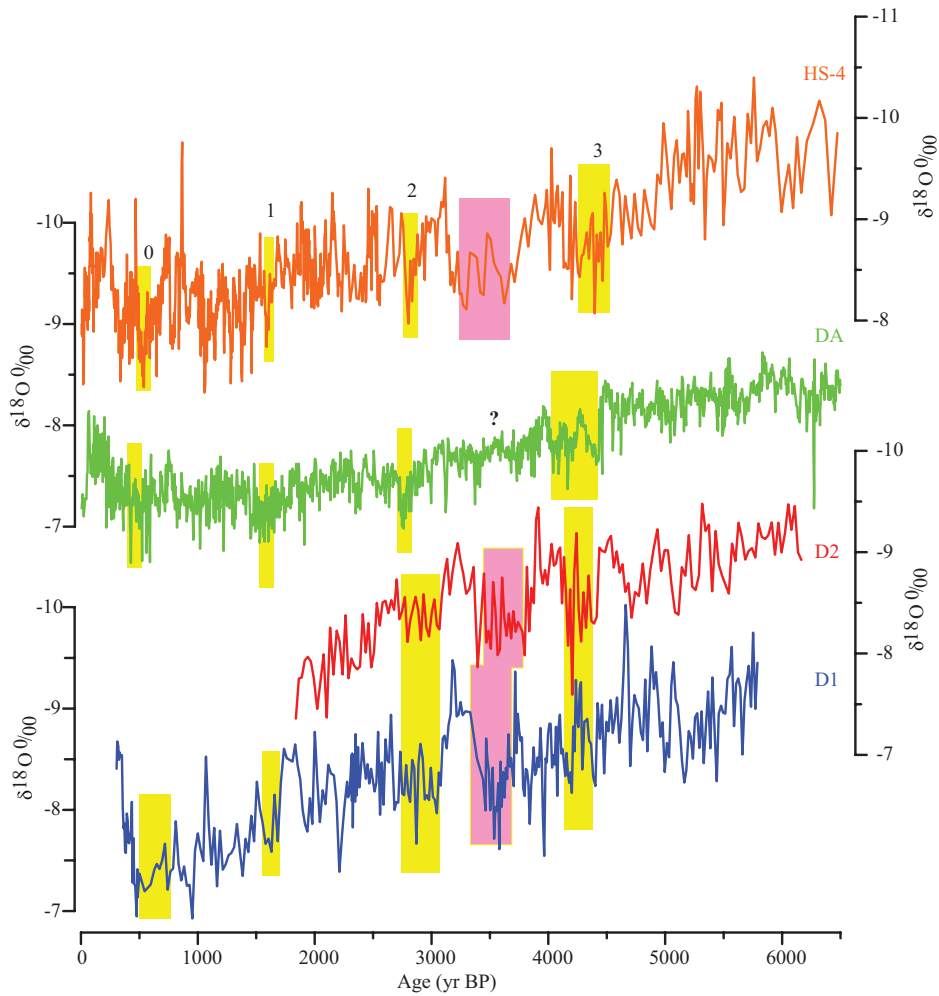


**Figure 7.**  $\delta^{18}\text{O}$  records of stalagmites D1 (blue) and D2 (red) from Dark Cave (this study), HS-4 (orange) from Heshang Cave (Hu et al., 2008) and DA (green) from Dongge Cave (Wang et al., 2005). Yellow bars denote the corresponding Bond Events in the North Atlantic and a pink bar shows a WM period at 3.7–3.4 kyr BP (see text) (colour figure available online).

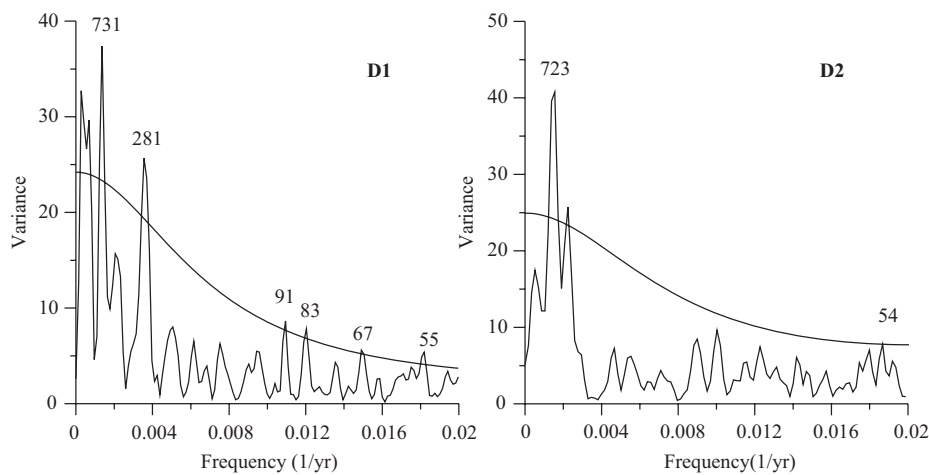


**Figure 8.** Spectral analysis of stalagmite D1 (left) and D2 (right)  $\delta^{18}\text{O}$  records using the Spectrum and Redfit spectral analysis program (Schulz and Mudelsee, 2002) for unevenly spaced paleoclimate data. Periodicities above the 95% confidence line are labeled.

North Atlantic (Bond et al., 1997), suggests this WM period did not result from high-latitude forcings.

Spectral analysis of the Dark Cave stalagmite  $\delta^{18}\text{O}$  records is shown in Figure 8. Decadal periodicities are difficult to resolve because of the limitation of 16 yr subsampling resolution. The Dark Cave stalagmite  $\delta^{18}\text{O}$  records display significant

periodicities at the 95% confidence level at periods centered on 731–723, 281, 91–83, 67, and 55–54 yr/cycles (Figure 8). The significant 731–723 yr cycle was observed in the South China Sea (Wang et al., 1999), tropical Indian Ocean (von Rad et al., 1999), and tropical central Africa (Russell et al., 2003). This cycle has been considered an intrinsic feature in the Holocene

tropical monsoon climate and could be a result of long-term changes in tropical sea surface temperature and the interaction with the tropical monsoon (Russell et al., 2003). Variability of low-latitude El Niño-Southern Oscillation (ENSO) could drive this 731–723 yr/cycle monsoon dynamics (Russell et al., 2003). Considering the frequency resolution (6 dB bandwidth) and the additional uncertainty of the age model, the 281 yr, 91–83 yr, 67 yr, and 55–54 yr cycles are close to significant periodicities of the  $\Delta^{14}\text{C}$  record (~288 yr, 88 yr, 68 yr, and ~57 yr (Damon and Peristykh, 2000)). Our data suggest that solar changes may be partly responsible for centennial–decadal changes in Holocene AM intensity, proposed by previous Chinese cave studies (e.g. Cai et al., 2008; Wang et al., 2005).

## Conclusions

The highly reproducible  $\delta^{18}\text{O}$  records from two stalagmites, D1 and D2, recovered from Dark Cave in southwest China reveal a detailed record of the features of the Asian Summer Monsoon system during the mid to late Holocene. The agreement of trends in the  $\delta^{18}\text{O}$  records from different regions of the Asian Monsoon supports the previous suggestion that solar insolation at 30°N is the primary forcing for ASM intensity for this time window. Dark Cave records reveal five centennial-scale weak monsoon periods, which reveal intrinsic characteristics of AM variability for the past 6 kyr. The results of our spectral analysis reveal that similar periodicities with solar variability records which may have influenced AM intensity on centennial to decadal periodicities since the mid Holocene.

## Acknowledgements

The authors thank C-C Wu for his laboratory assistance and X Kong for his suggestive discussion. Our thanks also to KL Delong, and D Scholz for useful comments and discussions. Comprehensive reviews by two anonymous reviewers significantly improved this paper.

## Funding

This study was supported by the National Natural Science Foundation of China (41002061) and the Natural Science Foundation of Fujian Province (2010J05093). Funding was also provided by Taiwan NSC grants (NSC 99-2611-M-002-006, 99-2628-M-002-012, and 100-3113-M-002-002 to C-CS)

## References

- An CB, Tang L, Barton L et al. (2005) Climate change and cultural response around 4000 cal yr B.P. in the western part of Chinese Loess Plateau. *Quaternary Research* 63: 347–352.
- An ZS, Porter SC, Kutzbach JE et al. (2000) Asynchronous Holocene optimum of the East Asian monsoon. *Quaternary Science Reviews* 19: 743–762.
- Anderson DM, Overpeck JT and Gupta AK (2002) Increase in the Asian Southwest Monsoon during the past four centuries. *Science* 279: 596–599.
- Berger A and Loutre MF (1991) Insolation values for the climate of the last 10 million years. *Quaternary Science Reviews* 10: 297–317.
- Bond G, Showers W, Cheseby M et al. (1997) A pervasive millennial-scale cycle in North Atlantic. *Science* 278: 1257–1266.
- Cai BG, Edwards RL, Cheng H et al. (2008) A dry episode during the Younger Dryas and centennial-scale weak monsoon events during the early Holocene: A high-resolution stalagmite record from southeast of the Loess Plateau, China. *Geophysical Research Letters* 35: L02705, doi: 10.1029/2007GL030986.
- Cai YJ, Tan LC, Cheng H et al. (2010) The variation of summer monsoon precipitation in central China since the last deglaciation. *Earth Planetary Science Letters* 291: 21–31.
- Cheng H, Edwards RL, Broecker WS et al. (2009) Ice age terminations. *Science* 326: 248–252.
- Cheng H, Edwards RL, Hoff J et al. (2000) The half-lives of uranium-234 and thorium-230. *Chemical Geology* 169: 17–33.
- Cheng H, Fleitmann D, Edwards RL et al. (2009) Timing and structure of the 8.2 kyr B.P. event inferred from  $\delta^{18}\text{O}$  records of stalagmites from China, Oman, and Brazil. *Geology* 37: 1007–1010.
- Cheng H, Sinha A, Wang XF et al. (2012) The global paleomonsoon as seen through speleothem records from Asia and the Americas. *Climate Dynamics* 39(5): 1045–1062.
- Damon PE and Peristykh AN (2000) Radiocarbon calibration and application to geophysics, solar physics, and astrophysics. *Radiocarbon* 42: 137–150.
- Dayem KE, Molnar P, Battisti DS et al. (2010) Lessons learned from oxygen isotopes in modern precipitation applied to interpretation of speleothem records of paleoclimate from eastern Asia. *Earth Planetary Science Letters* 295: 219–230.
- Dong JG, Wang YJ, Cheng H et al. (2010) A high-resolution stalagmite record of the Holocene East Asian monsoon from Mt Shennongjia, central China. *The Holocene* 20: 257–264.
- Dorale J and Liu ZH (2009) Limitations of Hندی Test criteria in judging the paleoclimatic suitability of speleothems and the need for replication. *The Journal of Cave and Karst Studies* 71: 73–80.
- Dykoski CA, Edwards RL, Cheng H et al. (2005) A high-resolution, absolute-dated Holocene and deglacial Asian monsoon records from Dongge cave, China. *Earth Planetary Science Letters* 233: 71–86.
- Fleitmann D, Burns SJ, Mangini A et al. (2007) Holocene ITCZ and Indian monsoon dynamics recorded in stalagmites from Oman and Yemen (Socotra). *Quaternary Science Reviews* 26: 170–188.
- Fleitmann D, Burns SJ, Mudelsee M et al. (2003) Holocene forcing of the Indian monsoon recorded on a stalagmite from southern Oman. *Science* 300: 1737–1739.
- Fleitmann D, Burns SJ, Neff U et al. (2004) Palaeoclimatic interpretation of high-resolution oxygen isotope profiles derived from annually laminated speleothems from Southern Oman. *Quaternary Science Reviews* 23: 935–945.
- Fleitmann D, Mudelsee M and Burns SJ (2008) Evidence for a widespread climatic anomaly at around 9.2 ka before present. *Paleoceanography* 23: PA1102, doi:10.1029/2007PA001519.
- Frohlich C, Hornbach MJ, Taylor FW et al. (2009) Huge erratic boulders in Tonga deposited by a prehistoric tsunami. *Geology* 37: 131–134.
- Guo QR, Cai JN, Shao XM et al. (2003) Interdecadal variability of East-Asian summer monsoon and its impact on the climate of China. *Acta Geographica Sinica* 4: 569–576 (in Chinese).
- Gupta AK, Anderson DM and Overpeck JT (2003) Abrupt changes in the Asian southwest monsoon during the Holocene and their links to the North Atlantic Ocean. *Nature* 421: 354–356.
- He Y, Theakstone WH, Zhang ZL et al. (2004) Asynchronous Holocene climatic change across China. *Quaternary Research* 61: 52–63.
- Hندی CH (1971) The isotopic geochemistry of speleothems-I. The calculation of the effects of different modes of formation on the isotopic composition of speleothems and their applicability as palaeoclimatic indicators. *Geochimica et Cosmochimica Acta* 35: 801–824.
- Hong YT, Hong B, Lin QH et al. (2005) Inverse phase oscillations between the East Asian and Indian ocean summer monsoons during the last 12000 years and paleo-El Niño. *Earth and Planetary Science Letters* 231: 331–346.
- Hu CY, Henderson GM, Huang JH et al. (2008) Quantification of Holocene Asian monsoon rainfall from spatially separated cave records. *Earth and Planetary Science Letters* 266: 221–232.
- IAEA/WMO (2006) *Global Network of Isotopes in Precipitation. The GNIP Database*. Accessible at: <http://www.iaea.org/water>.
- Jaffey AH, Flynn KF, Glendenin LE et al. (1971) Precision measurement of half-lives and specific activities of U-235 and U-238. *Physical Review* 4: 1889–1906.
- Jiang WY, Guo ZT, Sun XJ et al. (2006) Reconstruction of climate and vegetation changes of Lake Bayanchagan (Inner Mongolia): Holocene variability of the East Asian monsoon. *Quaternary Research* 65: 411–420.
- Jiang XY, He YQ, Shen C-C et al. (2012) Stalagmite-inferred Holocene precipitation in northern Guizhou Province, China, and asynchronous termination of the Climatic Optimum in the Asian monsoon territory. *Chinese Science Bulletin* 57: 795–801.
- Jung SJA, Davies GR, Ganssen GM et al. (2004) Synchronous Holocene sea surface temperature and rainfall variations in the Asian monsoon system. *Quaternary Science Reviews* 23: 2207–2218.
- Kutzbach JE (1981) Monsoon climate of the early Holocene: Climate experiment with Earth's orbital parameters for 9000 years ago. *Science* 214: 59–61.
- Lachniet M (2009) Climatic and environmental controls on speleothem oxygen-isotope values. *Quaternary Science Reviews* 28: 412–432.
- Liu DB, Wang YJ, Cheng H et al. (2010) Sub-millennial variability of Asian monsoon intensity during the early MIS3 and its analogue to the ice age terminations. *Quaternary Science Reviews* 9–10: 1107–1115.
- Liu G, Zhao P and Zhou XJ (2011) East Asian-North Indian Ocean thermal contrast and variation in the East Asian summer monsoon for the past 2650 years. *Science of China Earth Sciences* 54: 773–779.
- Liu J, Wang B and Yang J (2008) Forced and internal modes of variability of the East Asian summer monsoon. *Climate of Past* 4: 225–233.



- Neff U, Burns SJ, Mangini A et al. (2001) Strong coherence between solar variability and the monsoon in Oman between 9 and 6 ka ago. *Nature* 411: 290–293.
- Overpeck J and Cole J (2008) The rhythm of the rain. *Nature* 451: 1061–1063.
- Pausata FSR, Battisti DS, Nisancioglu KH et al. (2011) Chinese stalagmite  $\delta^{18}\text{O}$  controlled by changes in the Indian monsoon during a simulated Heinrich event. *Nature Geoscience* 4: 474–480.
- Russell JM, Johnson TC and Talbot MR (2003) A 725 yr cycle in the climate of central Africa during the late Holocene. *Geology* 31: 677–680.
- Scholz D and Hoffmann DL (2011) StalAge – An algorithm designed for construction of speleothem age models. *Quaternary Geochronology* 6: 369–382.
- Schulz M and Mudelsee M (2002) REDFIT: Estimating red-noise spectra directly from unevenly spaced paleolimatic time series. *Computers and Geosciences* 28: 421–426.
- Shao XH, Wang YJ, Cheng H et al. (2006) Long-term trend and abrupt events of the Holocene Asian monsoon inferred  $\delta^{18}\text{O}$  record from Shennongjia in Central China. *Chinese Science Bulletin* 51: 221–228.
- Shen C-C, Cheng H, Edwards RL et al. (2003) Measurement of attogram quantities of  $^{231}\text{Pa}$  in dissolved and particulate fractions of seawater by isotope dilution thermal ionization mass spectroscopy. *Analytical Chemistry* 75: 1075–1079.
- Shen C-C, Edwards RL, Cheng H et al. (2002) Uranium and thorium isotopic and concentration measurements by magnetic sector inductively coupled plasma mass spectrometry. *Chemical Geology* 185: 165–178.
- Shen C-C, Li K-S, Sieh K et al. (2008) Variation of initial  $^{230}\text{Th}/^{232}\text{Th}$  and limits of high precision U-Th dating of shallow-water corals. *Geochimica et Cosmochimica Acta* 72: 4201–4223.
- Shen C-C, Wu C-C, Cheng H et al. (2012) High-precision and high-resolution carbonate  $^{230}\text{Th}$  dating by MC-ICP-MS with SEM protocols. *Geochimica et Cosmochimica Acta* 99: 71–86.
- Sinha A, Stott L, Berkelhammer M et al. (2011) A global context for megadroughts in monsoon Asian during the past millennium. *Quaternary Science Reviews* 30: 47–62.
- Tan LC, Cai YJ, An ZS et al. (2011) Centennial- to decadal-scale monsoon precipitation variability in the semi-humid region, northern China during the last 1860 years: Records from stalagmites in Huangye Cave. *The Holocene* 21: 287–296.
- Tan LC, Cai YJ, Cheng H et al. (2009) Summer monsoon precipitation variations in central China over the past 750 years derived from a high-resolution absolute-dated stalagmite. *Palaeography, Palaeoclimatology, Palaeoecology* 280: 432–439.
- Tao SY and Chen L (1987) A review of recent research on East Asian summer monsoon in China. In: Chang CP and Krishnamurti TN (eds) *Monsoon Meteorology*. Oxford: Oxford University Press, pp. 60–92.
- von Rad U, Schaaf M, Michels KH et al. (1999) A 5000-yr record of climate changes in varved sediments from the oxygen minimum zone off Pakistan, northeastern Arabian Sea. *Quaternary Research* 51: 39–53.
- Wang B and Lin H (2002) Rainy season of the Asian-Pacific summer monsoon. *Journal of Climate* 15: 386–396.
- Wang B, Clemens SC and Liu P (2003) Contrasting the Indian and East Asian monsoons: Implications on geologic timescales. *Marine Geology* 201: 5–21.
- Wang L, Sarnthein M, Erlenkeuser H et al. (1999) East Asian monsoon climate during the late Pleistocene: High resolution sediment records from the South China Sea. *Marine Geology* 156: 245–284.
- Wang YJ, Cheng H, Edwards RL et al. (2001) A high-resolution absolute-dated late Pleistocene monsoon record from Hulu Cave, China. *Science* 294: 2345–2348.
- Wang YJ, Cheng H, Edwards RL et al. (2005) The Holocene Asian monsoon: Links to solar changes and North Atlantic climate. *Science* 308: 854–857.
- Wanner H, Solomina O, Grosjean M et al. (2011) Structure and origin of Holocene cold events. *Quaternary Science Reviews* 30: 3109–3123.
- Wu WX and Liu TS (2004) Possible role of the ‘Holocene Event 3’ on the collapse of Neolithic Culture around the Central Plain of China. *Quaternary International* 117: 153–166.
- Yancheva G, Nowaczyk NR, Mingram J et al. (2007) Influence of the inter-tropical convergence zone on the East Asian monsoon. *Nature* 445: 74–77.
- Zhang DE, Li HC, Ku TL et al. (2010) On linking climate to Chinese dynastic change: Spatial and temporal variations of monsoonal rain. *Chinese Science Bulletin* 55: 77–83.
- Zhang PZ, Cheng H, Edwards RL et al. (2008) A test of climate, sun, and culture relationships from an 1810-year Chinese cave record. *Science* 322: 940–942.